Laser Cutting of Polymer Templates for Water-Droplet Induced Self-Folding of Cubes: Hinge Geometry Optimization

Pierre Lorenz[1,*], Ronald Franz[2], Martin Ehrhardt[1], Gregory Lecrivain[2], Robert Kirchner[3], and Klaus Zimmer[1]

[1]*Leibniz Institute of Surface Engineering (IOM), Permoserstr. 15, D-04318 Leipzig, Germany*
[2]*Helmholtz-Zentrum Dresden-Rossendorf, Institut für Fluiddynamik, Bautzner Landstraße 400, 01328 Dresden, Germany*
[3]*Center for Advancing Electronics Dresden, TU Dresden, Helmholtzstraße 18, 01069 Dresden, Germany*
**Corresponding author's e-mail: pierre.lorenz@iom-leipzig.de*

Droplet-induced self-folding processes enable the easy and cost-effective fabrication of millimeter to submillimeter 3D structures from planar templates. These templates were fabricated by laser cutting of polymer foils that offer a high flexibility in design. The interaction of water droplets with template surfaces induces a surface tension force that causes the deformation of the laser-cut templates needed to form the 3D structures. In this study, laser patterning of 25 µm thick polyimide (PI) foils by UV ultrashort pulse laser ablation was used to systematically investigate the effect of hinge geometry on the bending and self-folding process of cubes. The deposition of water droplets on the laser-structured samples leads to forces that move the side faces of the cube template causing a defined deformation of the hinges of the PI template and resulting in a bending angle between hinged template regions. The bending angle was determined as a function of hinge geometry and water droplet volume. The bending angle is increased with increasing droplet volume below a certain maximum but decreased with increasing hinge thickness and width. Finally, 2D laser cut templates with optimized v-shaped hinge structures was sucessful formed into a cube by laser droplet induced self folding.

DOI: 10.2961/jlmn.2023.02.2001

Keywords: ps-laser; laser cutting, self-folding, water droplet, polyimide

1. Introduction

3D microstructures have a growing impact applications, e.g., in of the field of microelectronics [1]. Technical advances in the micro/nanofabrication technologies allow a rapid progress in the field of micro/nano-electromechanical systems (MEMs/NEMs) [2] and smart medical devices [3, 4] where the miniaturization and multifunctionality is an important issue. The folding of 2D patterns into functional 3D microstructures is a promising strategy for the cost-effective 3D microstructure fabrication along with functional integration [5]. Due to the micron size of the final structures, self-folding processes without complex external actuation are needed, which require highly accurate 2D templates including moveable part such as hinges. To initiate the self-folding process, forces must be provided to trigger the folding of the 2D template. Both, external and internal forces like capillary force [6-8] magnetic force [9, 10], ion/electron bombardment [11-13], strain gradient [14] and mismatch of mechanical properties in multi-layer stacks [15-17] has been utilized for folding processes. Especially capillary forces induced by surface tension of, e.g., water droplets enable easy and cost-effective self-folding processes of 2D templates with minimal impact on the device [18]. The usage of short and ultra-short laser pulses allows the fast, precise and flexible laser structuring of polymer surfaces by laser ablation [19-26]. The laser ablation process was studied for different polymers like polyimide (PI), polyethylene terephthalate (PET), polycarbonate (PC), polytetrafluoroethylene (PTFE) and polyether ether ketone (PEEK [19, 27]. Laser irradiation of the polymers can result in the decomposition of the material due to the disintegration of hydrocarbon chains by photothermal or photochemical processes [22]. The optical, chemical, thermal and electrical properties of polyimide qualify the polymer for various applications [27]. The laser ablation of PI was studied at pulse durations from femtosecond (fs) to nanosecond (ns) and at different wavelengths from UV to IR [21, 24, 25, 28, 29]. In this study, laser machining of PI was studied in relation to the geometry and the material modification for template fabrication for origami structures enabling water-droplet-induced self-folding. Therefore, the effect of laser machining to the mechanics of the hinge structures was analysed to optimize their geometry and demonstrate the self-folding of laser-machined 2D PI templates into cubes in the second part. The optimization target for the water droplet-induced bending angle is 90 ° as a successful self-folding of a cube is envisaged.

2. Experimental Setup

Hinge structures and 2D templates for micron-scale cubes were fabricated by laser ablation of 25 µm thin polyimide (PI, Kapton HN) foils. The general setup for laser cutting and machining is described elsewhere [30]. Laser machining by laser ablation of the PI foils was performed with a ps - laser (wavelength $\lambda = 355$ nm, pulse duration $\Delta t_p = 12$ ps, repetition rate f = 100 kHz). The laser beam was moved over the foil surface under computer control using a galvano scanner unit that includes an f-theta lens with a focal length of 103 mm to focus the Gaussian laser beam to a spot size of ~ 24 µm.

2.1 Fabrication and analysing of hinge structures

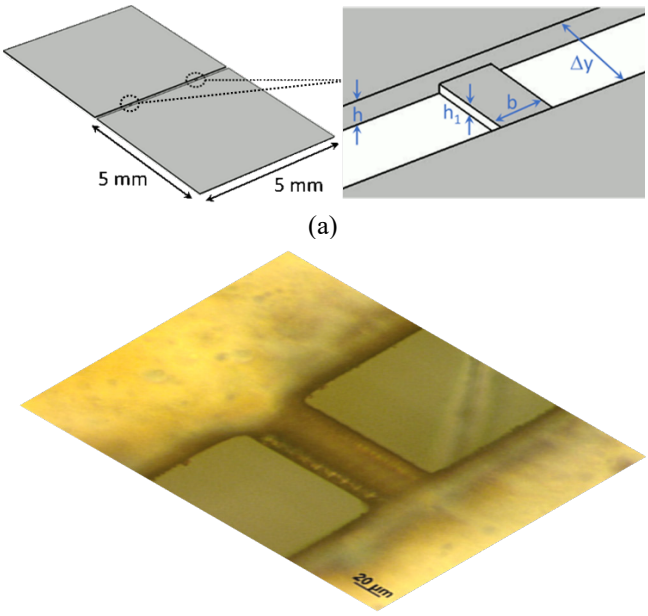

(a)

(b)

Fig. 1 (a) Sketch of the hinge test samples, (b) Exemplary microscopic image of a thinned hinge structure.

For the studies of the hinge structure and their optimization, hinge test samples consisting of two flaps that representing the faces of the cube being connected by hinges were produced. The layout of these samples is shown in Fig. 1 (a) with a hinge geometry defined by length Δy, thickness h_1, and width b.

The laser cutting of the PI foil for all samples was performed at a laser power of P = 200 mW, a scanning speed of v = 500 mm/s and number of transitions $N_t = 130$.

For the hinge structures, the PI foil was thinned by laser ablation along scan lines having a lateral distance of 10 µm which results in removing a specific PI layer thickness. Therefore, a laser power P ~ 150 mW and a scanning speed v = 200 mm/s were used. The laser parameter used are summarized in Tab. 1.

Table 1 Summary of the laser parameter used

	P [mW]	v [mm/s]	N_t
Laser cut	200	500	130
Laser thinning	150	200	1-7

The desired hinge thickness h_1 was adjusted by the number of transitions of removed PI layers. An exemplary microscopic image of a thinned hinge structure is shown in Fig. 1(b).

For the hinge studies, one flap of the samples (see Fig. 1) was clamped and the bending was determined from side-view images. For the droplet-induced self-folding tests of micron-scale cubes, the laser cut 2D PI templates were fixed on superhydrophobic stainless steel [31] and a defined volume of DI water was applied with a precision pipette at room temperature.

The laser-machined PI was imaged by optical microscopy (OM). Furthermore, the shape and the thickness of the hinge structures were analysed by white light interference microscopy (WLIM). SEM images were taken also. To eliminate any charging effect, the PI was magnetron sputtered with a thin gold layer. The water contact angle of pristine PI foils was determined to be $\varphi_{H2O} = (77.5 \pm 3)°$ using the sessile drop method [32]. Images and movies of the self-folding process of 2D templates after the water droplet application were taken with a camera with 30 fps.

2.2 Fabrication of 2D templates and self-folding

2D polyimide templates with before optimized hinge structures were produced by laser ablation. The laser cutting was performed with same parameter set but the optimized hinge geometry and processing strategy (based on the results of the first studies) were applied. The shape of the hinges used in the water-droplet induced self-folding was adapted based on the hinge structure tests. An exemplary 2D template for micron-scale cubes is shown in Fig. 2.

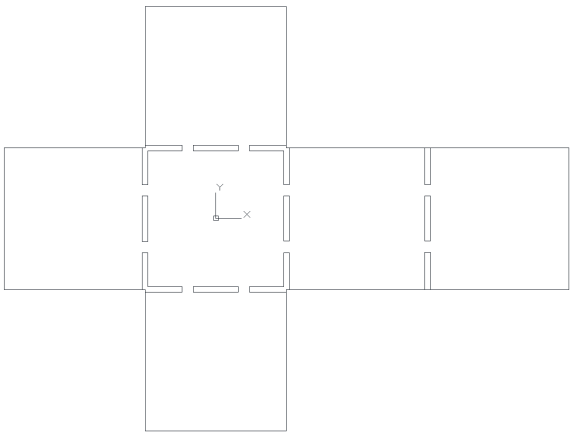

Fig. 2 CAD sketch of a 2D template for self-folding cubes in the mm to micron range.

3. Experimental results and Discussion

First the design and the mechanics of the hinges was studied for their optimization. Both the bending angle of hinge test samples in dependence on the hinge geometry (hinge thickness h_1, hinge width) were measured for gravity forces and after water droplet deposition for gravity and surface tension forces.

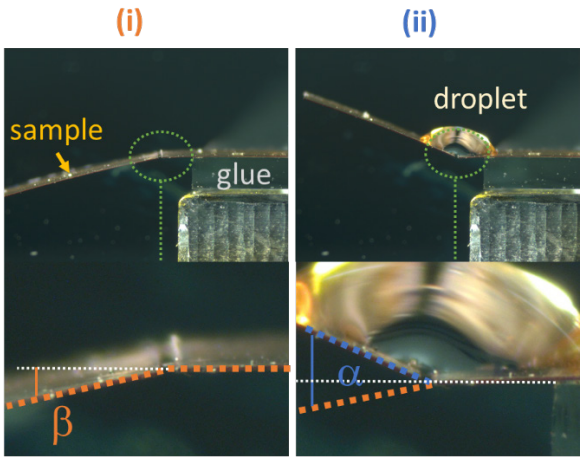

Fig. 3 Microscopic images of the state of initial laser structured PI and water droplet-induced state; (i) gravity (initial) and (ii) surface tension bending (with droplet of a volume about 1 µl).

3.1 Fabrication and analyzing of hinge structures

Side view images of the hinge test samples without and after applying a water droplet are shown in Fig. 3 which are referred to as gravity and surface tension bending, respectively. As seen, gravity causes a negative bending angle β due to the mass of the flap that induces a torque to the hinges (see Fig. 3 (i)). With the water droplet the surface tension results in the alteration of the bending with an angle α in the positive direction (see Fig. 3 (ii)).

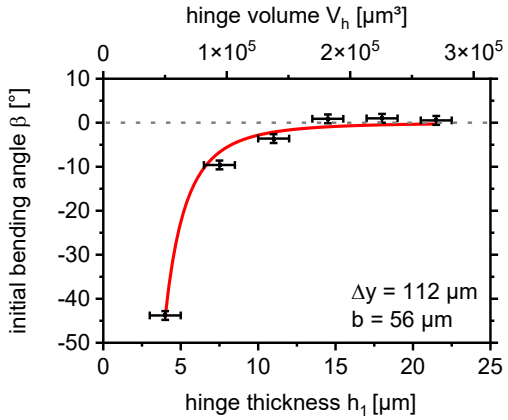

Fig. 4 Gravity induced initial bending angle α dependent on the hinge thickness (black square: measurements, red line: fit based on Eq. (1))

The bending due to gravity, as well as the surface tension of the hinge test samples, was studied depending on the hinge geometry (h_1, b) as well as on the water droplet volume. In general, the bending angles (α, β) due to gravity or surface tension of water droplets increase with thinner and smaller hinges as expected by the Euler–Bernoulli beam theory.

Especially hinge structures with a low thickness h_1 feature a gravity-induced initial bending (see (i) in Fig. 3). For hinges (two hinges per flap) with a hinge volume $V_h = 2 \cdot h_1 \cdot b \cdot \Delta y$ lower than $\sim 1.6 \cdot 10^5$ µm³ or a hinge thickness h_1 below 13 µm, the gravity causes a significant bending angle (see Fig. 4). Considering the gravitation induced bending angle is given by:

$$\beta = -\frac{3 \cdot \Delta y}{2 \cdot E \cdot b \cdot h_1^3} \cdot \rho \cdot g \cdot c^3 \cdot h = -\frac{-7.6 \cdot 10^{-7}\,^{\circ} kg \cdot m}{E \cdot h_1^3} \qquad (1)$$

with the density ρ, the gravity g, the flap edge size c and the Young's modulus E. From the fit of the experimental

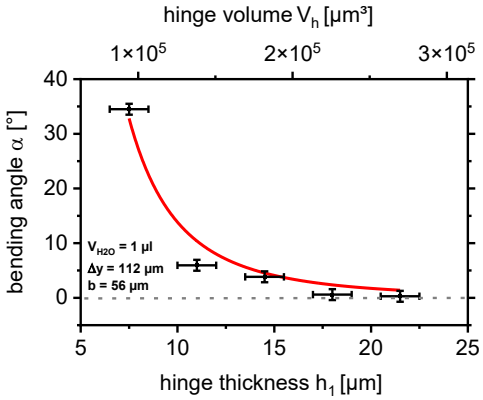

(a)

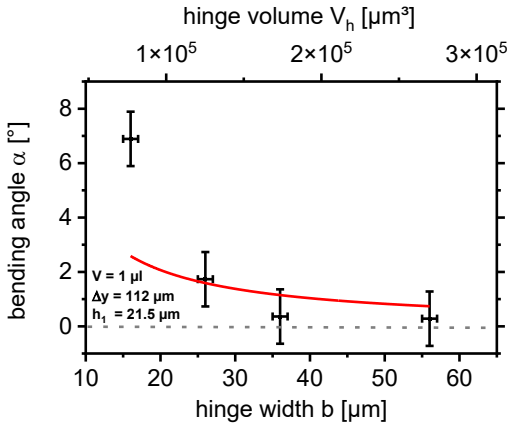

(b)

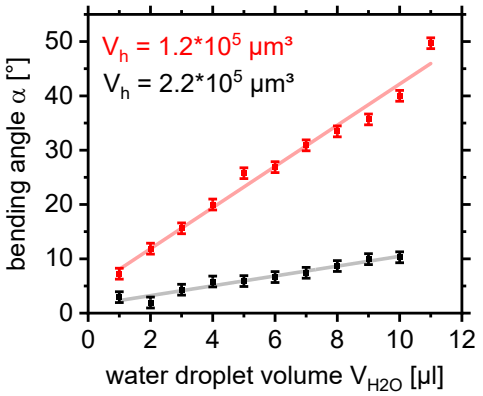

(c)

Fig. 5 Water contact induced bending angle α dependent on the hinge thickness h_1 (a) and the hinge width (b) at a water droplet volume of V_{H2O} = 1 µl, respectively. (black square: measurement, red curve: fit Eq. 2).
(c) Water droplet induced bending angle a dependent on the water droplet volume V_{H2O} (red/black square: measurement, red/black line: linear fit guide for the eye) of two selected hinge structures with $V_h = 1.2*10^5$ µm³ (h_1 = 13.1 µm, Δy = 105 µm, b = 45 µm) and $V_h = 2.2*10^5$ µm³ (h_1 = 11.1 µm, Δy = 105 µm, b = 95 µm).

data, see Fig. 4, to Eq. (1), the modulus of the PI hinges has been calculated to be $E = (2.69 \pm 0.11) \cdot 10^8$ Pa. The Young's modulus of these laser fabricated hinges is smaller than the Young's modulus of bulk PI that is in the range of 3 GPa [33]. In general, the degradation of polymers due to UV, heating or laser irradiation is well known [33-35]. Especially carbonization of the polyimide surface can influence the young's modulus.

For 50 µm thick polymer films the UV-irradiation induced reduction of the Young's modulus accounts for 10% [33]. In agreement with former studies on incubation effects at laser ablation, the heat and UV stress of the polyimide during the laser ablative pattering process induce chemical and structural alteration of the polymer within the laser-exposed polymer depth. Hence, secondary processes of the laser ablation can result in modifications of remaining polyimide (hinge structure) which can explain the determined reduced modified Young's modulus.

Applying a water-droplet on top of these samples results in upward bending of the flap as seen in Fig. 3 (ii). The dependence of the bending angle α change due to the surface tension is shown in Fig. 5

The bending angle α is almost linear to the water droplet volume V_{H2O} (see Fig. 5 (c)). Further, the experimental results implied that the slope of the bending angle – water droplet volume decreased at increasing hinge volume (see Fig. 5 (c)).

The increasing of the water droplet volume result in an increasing of the contact area. At a water contact angel of $\theta = 77.5°$ and under assumption of a rigid substrate the water droplet area A_{H2O} can be described by:

$$A_{H2O} = \pi \cdot \left(sin\theta \cdot \sqrt[3]{\left(\frac{3 \cdot V_{H2O}}{\pi \cdot (2+cos\theta)}\right) \cdot (1-cos\theta)^2} \right)^2 \quad (2)$$

The increase in the water contact area and the contact volume leads to an increase in the torque and therefore to an increase in the bending angle.

Furthermore, the bending angle α increases with reduced hinge cross section (width and thickness) (see Fig. 5 (a) & (b)). In addition to the experimental data shown in Fig. 5, fitted curves to a beam theory-based model (see Eq. (3)) are shown. The approximation given in Eq. (3) considers in addition to the gravity the torque caused by the surface tension M_{ST}.

$$\alpha = \frac{3 \cdot \Delta y}{E \cdot b \cdot h_1^3} \cdot \left(M_{ST} - M_g\right) \quad (3)$$

For a water volume of 1 µl an effective torque M of $M = (3.26 \pm 0.08)\ 10^{-8}$ Nm can be estimated. The impact of the hinges width to the bending has been studied for gravity and surface tension also; with reducing the hinges width larger angles were measured.

Within the experiments, it has been found that sometimes the hinges were broken for large bending angles. The issue has been solved by modification of the hinge's shape by optimization of the machining strategy.

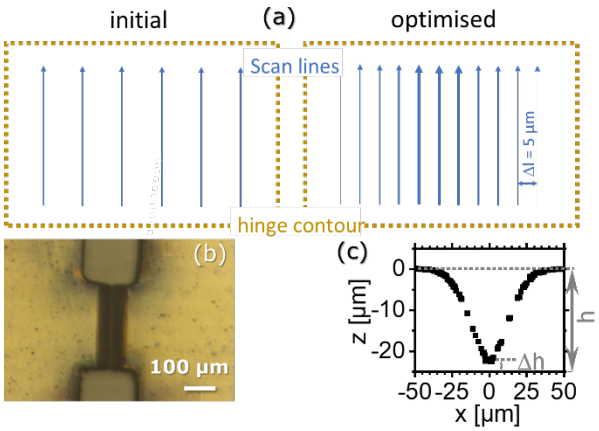

Fig. 6 (a) Laser machining strategy for the shaping the cross section of stable hinge structures (The thickness of the lines schematic illustrated the number of transitions N_t (thicker line higher N_t)).
(b) Microscopic image of hinge structure with optimised contour
(c) WLI line profile of optimised hinge structure.

In Fig. 6 (a) the initial and the optimized laser machining strategy are compared as well as in Fig. 8 a microscopic image of the complete laser cut 2D template is shown. The cross section of the hinges changes as seen in Fig. 6 (c) to a rather V-shape.

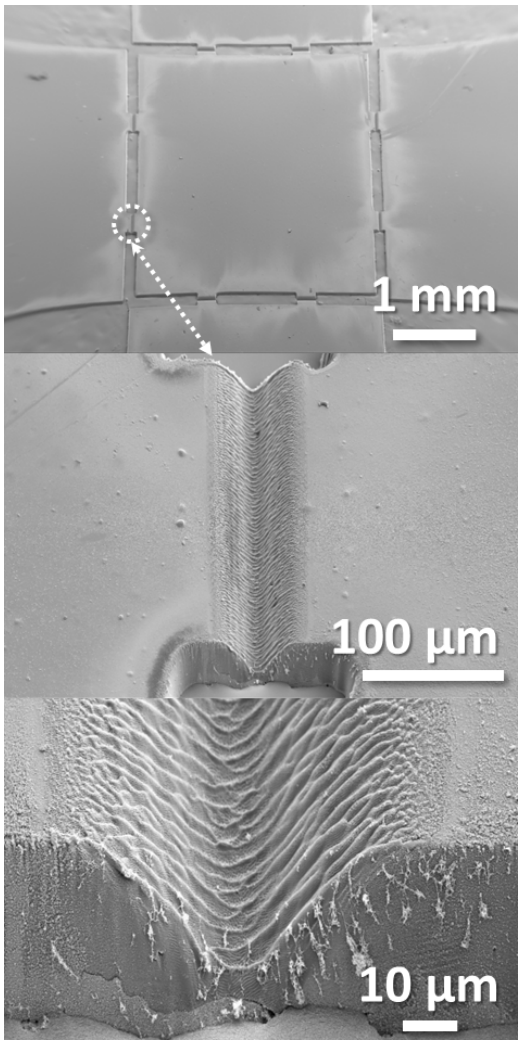

Fig. 7 SEM images of laser fabricated hinge structure

Slightly adapted laser processing parameters were used: distance of Δl = 5 µm, a laser power of 200 mW and a scanning speed of 500 mm/s. As sketched in Fig. 6 (a), the number of laser scans applied for hinge thinning changed across the hinge length from 1 at the edges to 7 at the centre. The resulting hinges feature a well-defined V-shape with a thickness of 2.5 µm in the centre (see Fig. 6 (c)) that leads to a smoother stress distribution within the hinge to handle the large deformation. This causes the localization of the bending to the centre of the hinges and results in a well-defined bending geometry. The SEM images of the hinge structure are shown in Fig. 7. The laser treatment results in the distinct increasing of the surface roughness in the hinge structure. It can be assumed that the laser induced chemical and morphological changes in the hinge locally influence the water contact angle. However, the contact area of the hinge is two orders of magnitude smaller than the contact area with the cube surfaces, so that an influence on the folding process can be almost excluded.
In consequence, a random bending location is avoided which leads to the undesired result of a less-defined 3D shape formation by self-folding and the collision of adjacent faces during the folding process. This can result in additional forces that contribute to the overall stress in the hinges and can cause the failure of the hinges.

3.2 Fabrication of 2D templates and self-folding

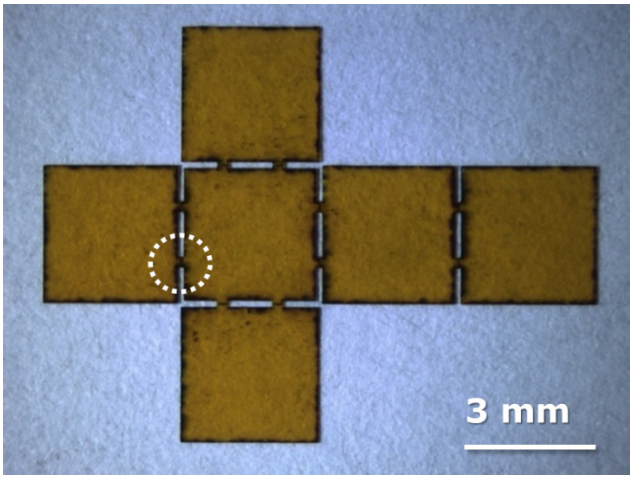

Fig. 8 Optical image of ps-laser-cut polyimide foil
The white circle frames a hinge structure (Optical image of laser-structured hinge structure, see Fig. 6 and 7).

For a complete self-folding of templates to cubes, folding angles exceeding 90° are necessary. With the optimized design features, the 2D template for the cube – the contour is seen in the CAD sketch of Fig. 2 –was complemented. The design was used to laser machine the 25 µm PI using the given parameters. An exemplary optical image of the laser structured 2D template is shown in Fig. 8. The 2D templates of the cubes were fixed to an antiadhesive, superhydrophobic steel to exclude the interaction of the water droplet with the whole substrate surface and allow only for the wetting of the upper side of the template. The manual application of a water droplet with a volume of ~27 µl by a pipette to the upper side of the 2D template results in a self-

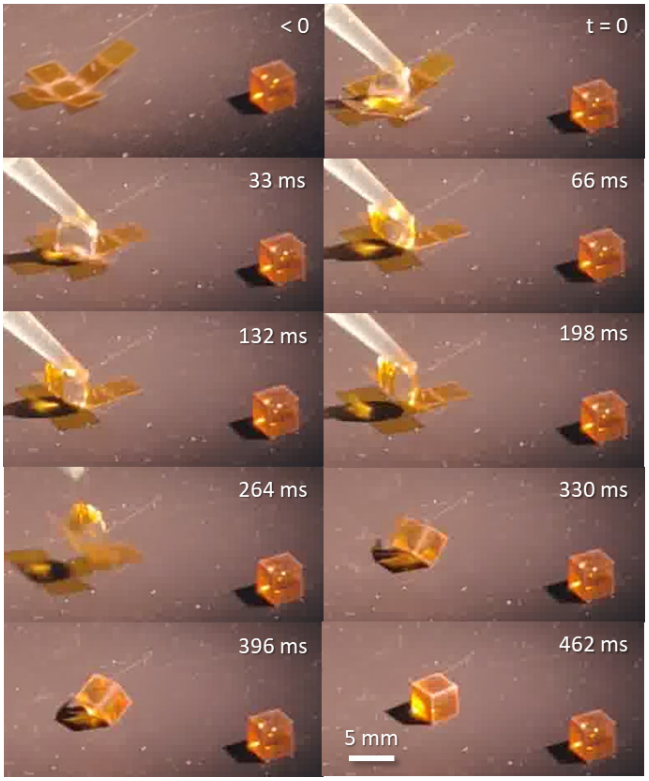

Fig. 9 Optical images of Water-droplet induced self-folding of 3D polyimide cube with an edge length of 3 mm.

folding into a 3D cube. A series of images extracted from videos of the self-folding process shows: first the application of the water droplet, the wetting the surface and the very fast folding process that is finished in less than 300 ms can be seen in Fig. 9. The individual facet fold even faster, within one range of one frame of the video and thus within 33 ms.

4. Conclusion and Outlook

The application of water droplets to a flexible laser-cut 2D template leads to a deformation of the template. The laser-based adjustment of the hinge structure geometry allows a well-defined tuning of the deformation and the bending angle. The bending angle increases with increasing droplet volume and decreases with increasing hinge thickness and width. For small hinge volumes (small width and thickness), gravity alone leads to a bending of the PI structure characterized by a downward bending angle. For water-droplet-induced formation of a cube structure from a laser-cut 2D template, i.e., a bending angle of at least 90°, a small hinge depth or hinge volume is required. Laser machined V-shaped hinge profiles meet these requirements with that self-folding of 3D cubes has been successfully demonstrated. The shown adjustability of the bending angle allows the fabrication of complex 3D structures based on laser-cut and structured 2D templates. As a guideline for the fabrication of laser cut 2D templates for successful water drop induced self-folding, it can be deduced from the results that for small target bending angles, homogeneously thinned hinges are very suitable as this allows a very precise adjustment of the bending angle. For large bending angles (≥90°), on the other hand, a V-shaped hinge is most

suitable, as this profile allows a large bending angle with sufficient mechanical stability at the same time.

Acknowledgements

This work was supported by the Deutsche Forschungsgemeinschaft (DFG) (Project No. 419981939 (KI 1980/6-1 and ZI 660/19-1, PlasCode) as well as No. 326062881 (KI 1980/1-1, KI 1980/8-1), M3SR).

References

[1] D. Karnaushenko, T. Kang, V.K. Bandari, F. Zhu, and O.G. Schmidt: Adv Mater, 32, (2020) 1902994.
[2] J. Rogers, Y. Huang, O.G. Schmidt, and D.H. Gracias: MRS Bulletin, 41, (2016) 123.
[3] Y. Huang, V. Fitzpatrick, N. Zheng, R. Cheng, H. Huang, C. Ghezzi, D.L. Kaplan, and C. Yang: Adv. Healthc. Mater., 9, (2020) 2000530.
[4] S.K. Srivastava, M. Medina-Sánchez, B. Koch, and O.G. Schmidt: Adv Mater, 28, (2016) 785.
[5] Y. Yu, P. Lorenz, C. Strobel, J. Zajadacz, M. Albert, K. Zimmer, and R. Kirchner: Small, 18 (2022) 10.
[6] K.S. Kwok, Q. Huang, M. Mastrangeli, and D.H. Gracias: Adv. Mater. Interfaces, 7, (2020) 1901677.
[7] X. Guo, H. Li, B. Yeop Ahn, E.B. Duoss, K.J. Hsia, J.A. Lewis, and R.G. Nuzzo: Proc. Natl. Acad. Sci. U.S.A., 106, (2009) 20149.
[8] S. Pandey, M. Ewing, A. Kunas, N. Nguyen, D.H. Gracias, and G. Menon: Proc. Natl. Acad. Sci. U.S.A., 108, (2011) 19885.
[9] J. Cui, T.Y. Huang, Z. Luo, P. Testa, H. Gu, X.Z. Chen, B.J. Nelson, and L.J. Heyderman: Nature, 575, (2019) 164.
[10] H. Xu, M. Medina-Sánchez, V. Magdanz, L. Schwarz, F. Hebenstreit, and O.G. Schmidt: ACS Nano, 12, (2018) 327.
[11] C. Dai, L. Li, D. Wratkowski, and J.-H. Cho: Nano Lett., 20, (2020) 4975.
[12] J.-H. Cho, M.D. Keung, N. Verellen, L. Lagae, V.V. Moshchalkov, P. Van Dorpe, and D.H. Gracias: Small, 7 (2011) 1943.
[13] C. Dai, and J.-H. Cho: Nano Lett., 21 (2021) 2066.
[14] M. Jamal, A.M. Zarafshar, and D.H. Gracias: Nature Communications, 2 (2011) 527.
[15] B. Bircan, M.Z. Miskin, R.J. Lang, M.C. Cao, K.J. Dorsey, M.G. Salim, W. Wang, D.A. Muller, P.L. McEuen, and I. Cohen: Nano Lett., 20, (2020) 4850.
[16] L. Ionov: Soft Matter, 7, (2011) 6786.
[17] G. Stoychev, N. Puretskiy, and L. Ionov: Soft Matter, 7, (2011) 3277.
[18] H. Li, X. Guo, R.G. Nuzzo, and K. Jimmy Hsia: J Mech Phys Solids, 58, (2010) 2033.
[19] A.A. Serafetinides, M.I. Makropoulou, C.D. Skordoulis, and A.K. Kar: Appl. Surf. Sci., 180, (2001) 42.
[20] S. Ravi-Kumar, B. Lies, X. Zhang, H. Lyu, and H. Qin: Polym. Int., 68, (2019) 1391.
[21] P. Lorenz, L. Bayer, M. Ehrhardt, K. Zimmer, and L. Engisch: Proc. SPIE, Vol. 9351, 2015, 935119.
[22] D. Bäuerle: "Laser Processing and Chemistry", (Springer, Berlin, Heidelberg, New York, 2011).
[23] P.E. Dyer: Applied Physics A, 77 (2003) 167-173.
[24] P.E. Dyer, M. Pervolaraki, and T. Lippert: Appl. Phys. A, 80, (2005) 529.
[25] J. Hrabovsky, C. Liberatore, I. Mirza, J. Sladek, J. Beranek, A.V. Bulgakov, and N.M. Bulgakova: Interfacial Phenom Heat Transf., 7 , (2019) 113.
[26] T. Lippert, M. Hauer, C.R. Phipps, and A. Wokaun: Appl. Phys. A, 77 (2003) 259.
[27] A. Lasagni, M. Cornejo, F. Lasagni, and F. Muecklich: Adv. Eng. Mater., 10, (2008) 488.
[28] I. Antanavičiūtė, L. Šimatonis, O. Ulčinas, A. Gadeikytė, B. Abakevičienė, S. Tamulevičius, V. Mikalayeva, V.A. Skeberdis, E. Stankevičius, and T. Tamulevičius: J Tissue Eng Regen Med, 12, (2018) e760.
[29] M. Ohnishi, H. Shikata, M. Sakakura, Y. Shimotsuma, K. Miura, and K. Hirao: Appl. Phys. A, 98, (2009) 123.
[30] P. Lorenz, M. Ehrhardt, and K. Zimmer: J. Laser Micro Nanoeng., 17 (2022) 6.
[31] P. Lorenz, J. Zajadacz, F. Marquardt, M. Ehrhardt, G. Hommes, S. Peter, and K. Zimmer: Procedia CIRP, 111, (2022) 711.
[32] D. Tiab, and E.C. Donaldson: “Petrophysics” , ed. By D. Tiab and E.C. Donaldson (Gulf Professional Publishing, Boston, 2012) p. 371.
[33] C. Qu, J. Hu, X. Liu, Z. Li, and Y. Ding: Materials, 10, (2017) 1329.
[34] D.S. Dunn and A.J. Ouderkirk: Macromolecules, 23 (1990) 770.
[35] N. Chidambaram, R. Kirchner, R. Fallica, L. Yu, M. Altana, and H. Schift: Adv. Mater. Technol., 2, (2017) 1700018.

(Received: April 5, 2023, Accepted: June 11, 2023)